The Dust Halo of Saturn's Largest Icy Moon, Rhea

G. H. Jones, *et al.*

Science **319**, 1380 (2008);
DOI: 10.1126/science.1151524

Science (print ISSN 0036-8075; online ISSN 1095-9203) is published weekly, except the last week in December, by the American Association for the Advancement of Science, 1200 New York Avenue NW, Washington, DC 20005.

knick-point propagation, lake overflow (*20*), or karst capture (*18*). Marble Canyon mammillaries also indicate fast incision rates. At river miles 57 (site 7) and 32 (site 8), incision rates are 166 and 374 m/My, respectively, and at river mile 38, a speleogenetic gypsum crust yielded a U-series age of 0.15 Ma at 50 m above the river and an incision rate of ≤330 m/My.

Even though our interpretation assumes no structural or hydrologic complexities, those complexities could help to explain any apparent inconsistencies as data accumulate. However, it is likely that the structure and hydrology will not change the overall interpretation that the western Grand Canyon is older than the eastern Grand Canyon. For instance, an explanation for the higher incision rate at site 1 (Bobcat Cave, Grand Wash Cliffs) could be the presence of an elevated water table north of the western Grand Canyon at 7.6 Ma. Even without this interpretation, the highest western Grand Canyon incision rate from the Grand Wash Cliffs mammillary of 123 m/My (site 1) is still less than the slowest incision rate for the eastern Grand Canyon (166 m/My, site 7; Fig. 3 and fig. S3C). The fast incision rate at Bedrock Canyon (site 8) indicates that 300 m of incision occurred in Marble Canyon over the past 1 My. However, at river miles 57 (site 7) and 60 (*19*), incision rates are slower (~140 to 230 m/My). Structure, hydrology, or headward erosion history (i.e., knick-point propagation from site 7 to site 8) might resolve these differences when additional data are available.

Overall, our data argue for an older Grand Canyon that was modified in the late Miocene by a fully integrated Colorado River that accelerated the headward erosion of the eastern Grand Canyon. We found that mammillary calcite is not restricted to large caves in the Redwall and Muav limestones, but also occurs in small fissure-controlled caves in other units such as the overlying Supai Formation. Hundreds of these deposits probably exist throughout the canyon, offering the potential for a reconstruction of the canyon's history, with a resolution perhaps high enough to explain complexities of the canyon's history related to faults, folds, and volcanic and tectonic activity.

References and Notes

1. W. Ranney, *Carving Grand Canyon—Evidence, Theories, and Mystery* (Grand Canyon Association, Grand Canyon, AZ, 2005).
2. K. E. Karlstrom *et al.*, *Geol. Soc. Am. Bull.* **119**, 1283 (2007).
3. A. L. Lange, *Plateau* **27**, 1 (1955).
4. T. C. Atkinson, P. J. Rowe, in *Uranium-Series Disequilibrium: Applications to Earth, Marine, and Environmental Sciences*, M. Ivanovich, R. Harmon, Eds. (Oxford Univ. Press, New York, 1992), pp. 669–703.
5. R. L. Edwards, J. H. Chen, G. J. Wasserburg, *Earth Planet. Sci. Lett.* **81**, 175 (1986).
6. C. A. Hill, P. Forti, *Cave Minerals of the World* (National Speleological Society, Huntsville, AL, 1997).
7. V. J. Polyak, C. A. Hill, Y. Asmeron, *GSA Abs. Prog.* **36**, 549 (2004).
8. I. J. Winograd *et al.*, *Science* **242**, 1275 (1992).
9. B. J. Szabo, P. T. Kolisar, A. C. Riggs, I. J. Winograd, K. R. Ludwig, *Quat. Res.* **41**, 56 (1994).
10. C. A. Hill, V. J. Polyak, W. C. McIntosh, P. P. Provencio, in *Colorado River Origin and Evolution*, R. A. Young, E. E. Spamer, Eds. (Grand Canyon Association, Grand Canyon, AZ, 2001), pp. 141–146.
11. See supporting material on *Science* Online.
12. D. A. Richards, S. H. Bottrell, R. A. Cliff, K. Strohle, P. J. Rowe, *Geochim. Cosmochim. Acta* **62**, 3683 (1998).
13. J. Woodhead *et al.*, *Quat. Geochronol.* **1**, 208 (2006).
14. J. E. Faulds, L. M. Price, M. A. Wallace, in *Colorado River Origin and Evolution*, R. A. Young, E. E. Spamer, Eds. (Grand Canyon Association, Grand Canyon, AZ, 2001), pp. 93–100.
15. L. S. Beard, *GSA Spec. Pap. 303*, 27 (1996).
16. J. E. Faulds, M. A. Wallace, L. A. Gonzalez, M. T. Heizler, in *Colorado River Origin and Evolution*, R. A. Young, E. E. Spamer, Eds. (Grand Canyon Association, Grand Canyon, AZ, 2001), pp. 81–87.
17. J. E. Spencer, L. Peters, W. C. McIntosh, P. J. Patchett, in *Colorado River Origin and Evolution*, R. A. Young, E. E. Spamer, Eds. (Grand Canyon Association, Grand Canyon, AZ, 2001), pp. 89–92.
18. C. A. Hill, N. Eberz, R. H. Buecher, *Geomorphology* **95**, 316 (2008).
19. J. Pederson, K. Karlstrom, W. Sharp, W. McIntosh, *Geology* **31**, e17 (2003).
20. N. Meek, J. Douglass, in *Colorado River Origin and Evolution*, R. A. Young, E. E. Spamer, Eds. (Grand Canyon Association, Grand Canyon, AZ, 2001), pp. 199–206.

21. Supported by NSF grant EAR-0518602 and by a National Park Service research grant. We thank E. Benenati and K. Voyles for the necessary collection permits; the Navajo, Hopi, and Hualapai tribes for permission to enter and collect from caves on their land; P. Provencio, A. Hill, C. Mosch, and M. Goar for field assistance; S. Davis, D. Powell, M. Oliphant, and N. Pistole for helping us to gain access to remote areas along the river; A. and P. Palmer for help in the field and through cave science discussions along the river; and especially B. and D. Buecher and D. Powell for their tremendous amount of fieldwork and sample elevation-location data.

Supporting Online Material

www.sciencemag.org/cgi/content/full/319/5868/1377/DC1
Materials and Methods
Figs. S1 to S3
Table S1
References

2 October 2007; accepted 30 January 2008
10.1126/science.1151248

The Dust Halo of Saturn's Largest Icy Moon, Rhea

G. H. Jones,[1,2,3]* E. Roussos,[1] N. Krupp,[1] U. Beckmann,[4] A. J. Coates,[2,3] F. Crary,[5] I. Dandouras,[6] V. Dikarev,[1,4,7] M. K. Dougherty,[8] P. Garnier,[6,9] C. J. Hansen,[10] A. R. Hendrix,[10] G. B. Hospodarsky,[11] R. E. Johnson,[12] S. Kempf,[4] K. K. Khurana,[13] S. M. Krimigis,[14,15] H. Krüger,[1] W. S. Kurth,[11] A. Lagg,[1] H. J. McAndrews,[2,19] D. G. Mitchell,[14] C. Paranicas,[14] F. Postberg,[4] C. T. Russell,[13] J. Saur,[16] M. Seiß,[17] F. Spahn,[17] R. Srama,[4] D. F. Strobel,[18] R. Tokar,[19] J.-E. Wahlund,[9] R. J. Wilson,[19] J. Woch,[1] D. Young[5]

Saturn's moon Rhea had been considered massive enough to retain a thin, externally generated atmosphere capable of locally affecting Saturn's magnetosphere. The Cassini spacecraft's in situ observations reveal that energetic electrons are depleted in the moon's vicinity. The absence of a substantial exosphere implies that Rhea's magnetospheric interaction region, rather than being exclusively induced by sputtered gas and its products, likely contains solid material that can absorb magnetospheric particles. Combined observations from several instruments suggest that this material is in the form of grains and boulders up to several decimetres in size and orbits Rhea as an equatorial debris disk. Within this disk may reside denser, discrete rings or arcs of material.

On 26 November 2005, Cassini encountered Rhea, the second largest of Saturn's moons, at 500 km altitude, detecting in situ the anticipated (*1*, *2*), approximately spherical distribution of grains lofted from its surface by interplanetary dust impacts. Cassini passed downstream of Rhea with respect to the local magnetospheric flow (Fig. 1) and observed the anticipated wake caused by plasma striking the moon, together with an unpredicted depletion of energetic electrons extending to ~8 Rhea radii (R_R) (Fig. 2). The scale of the depletion indicates that some material is absorbing electrons within the volume dominated by Rhea's gravitational field: its Hill sphere, of radius 7.7 R_R. Voyager 1 measurements in 1980 previously indicated a broadened depletion's presence farther downstream (*3*). A more distant Cassini flyby in August 2007 also showed evidence of a broad electron depletion (*4*). No such features have yet been observed at Dione and Tethys, but energetic electrons are absorbed by grains ejected from Enceladus's south pole (*5*). The signature's profile indicates that the electron-absorbing material has a near-symmetrical distribution about Rhea. No evidence was found by Cassini's instruments for the presence of large amounts of freshly ionized gas, which could theoretically scatter electrons. Neutral gas and dust populations are therefore the primary absorbing-medium candidates.

As Cassini passed Rhea, its cosmic dust analyzer (CDA) (*6*) registered an increase in the impact rate of >1 μm particles (Fig. 3), signaling the predicted envelopment of the moon (*1*, *2*) by dust ejected by micrometeoroids impacts. An impact-ejecta model (*1*) indicates a

preliminary interplanetary projectile flux of 5×10^{-15} kg m^{-2} s^{-1} (*4*), liberating ~230 kg s^{-1} of dust, corresponding to 7.2×10^{14} particles s^{-1} larger than 1 μm. CDA and radio and plasma wave science instrument (RPWS) detected a dust distribution sharply peaked near closest approach. The magnetospheric imaging instrument (MIMI) ion and neutral camera (INCA) recorded a flatter distribution extending beyond the Hill sphere, suggesting that it is most sensitive to small grains, and consequently that smaller Rhea impact ejecta have higher velocities. Unlike the electron signatures, there is no clear dust signal coincident with the Hill sphere boundary: The electron fluxes reflect the integrated effects of electrons' traverses of an absorbing medium before reaching Cassini's energetic electron detectors; most absorbing material is inferred to reside north of Cassini's path (*4*). Fluxes were slightly enhanced outbound in RPWS and MIMI-INCA data, when Cassini was nearest Rhea's equatorial plane.

Neutral gas surrounding Rhea is liberated from the moon and its dust halo through dust impacts and magnetospheric particle sputtering (*7*). Upper limits in column density deduced using the ultraviolet imaging spectrograph (UVIS) (*8*) are 1.5×10^{13} cm^{-2} for O and 1.6×10^{14} cm^{-2} for O_2. Independently derived MIMI-INCA upper limits (fig. S1) are sensitive to the assumed background ion flux; the upper limits for the same species are in the range of 10^{13} to 10^{14} cm^{-2} (see SOM text).

The quantity of electron-absorbing material can be estimated by gauging electron path lengths within the Hill sphere. Most <700 keV electrons observed by MIMI and the Cassini plasma spectrometer (CAPS) traverse the Hill sphere several times north-south before detection, bouncing along Saturn's convecting magnetic field lines (*9*). The reduced fluxes reflect the integrated effects of gas and dust upstream of Cassini's location ~200 km south of Rhea's equatorial plane. We modeled the effect of an electron-absorbing, spherically symmetric gas cloud required to produce the broad electron depletion. Implied neutral gas column densities of ~10^{18} cm^{-2} near Rhea's surface easily exceeded the column density upper limits. We next modeled a spherically symmetric dust halo, the densest possible based on CDA data, with number density falling off as an inverse power law with radial distance of –2.5 and a grain size of ~10 μm. Electron number densities were assumed to decrease by a factor of e^2 when the column mass encountered equaled the electrons' range in water (*10*, *11*). Coulomb collisions were excluded. There was no unique solution, but surface densities required were >2 orders of magnitude higher than implied by CDA data. The –2.5 density falloff is too steep to explain the detectable depletion at the Hill sphere's edge.

To explain the observations, the presence of an additional electron-absorbing obstacle is implied. An analysis of the electron data indicates that this obstacle is most likely in the form of a low optical depth disk of material near Rhea's equatorial plane and that the disk contains solid bodies up to ~1 m in size (*4*). Dynamical studies show that such bodies could orbit persistently near the equatorial plane. The disk explains the electron signature and is consistent with in situ data south of the equatorial plane, because Cassini did not traverse the plane itself. There have been no reports of remote observations of such a disk, but it would not be easy to detect (*4*). A weakly perceptible population of neutral gas and related products could also be present. Neutral gas is primarily lost through ionization and subsequent transport by the magnetospheric plasma. Several plasma measurements imply that there is a detectable, although not fully understood, interaction between Saturn's magnetosphere and freshly ionized material around Rhea, at the scales of the moon's Hill sphere (Fig. 2). As Cassini traversed the Hill sphere, electron number densities increased slightly at ~22:25 UT, near the inbound boundary, but a similar outbound feature is difficult to identify. Bulk velocities derived from the thermal plasma ion data shown in Fig. 2E were below corotation within the Hill sphere and displayed a ≤10° anti-Saturnward flow deviation inbound.

Several short-duration dips in MIMI low-energy magnetospheric measurement system (LEMMS) electron flux are also evident, lasting a few seconds each, or tens of km along the spacecraft track, and are nearly symmetrical about Rhea (Fig. 4). No plasma-related cause for these narrow electron dips has been identified. They are not believed to be electron phase-space holes, which usually result from a two-stream instability, as may occur in the wakes of absorbing bodies (*12*). Such structures are typically traversed in tens of milliseconds as opposed to several seconds. The dips are, however, consistent with additional obstacles residing upstream or directly north of Cassini, in Rhea's equatorial plane, that cause the occultation of electrons before detection at Cassini. The broadening of the dips with increasing electron energy (fig. S8) is as expected for an obstacle to electrons; the widening reflects electrons' larger gyroradii and slower convection through the Hill sphere at higher energies, and hence more prolonged absorption. The simplest explanation of these near-symmetrical features is that extended arcs or rings of material orbit Rhea

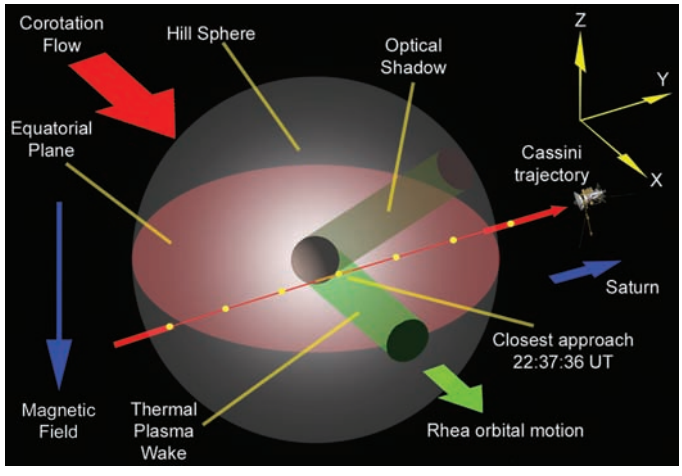

Fig. 1. Geometry of the 2005 flyby. Rhea is continuously overtaken at ~58 km s^{-1} by cold Saturnian magnetospheric plasma (*7*) flowing in the direction of the moon's orbital motion. Cassini's path through Rhea's Hill sphere was downstream of the moon with respect to this flow, entering at 22:24:39 when 290 km south of the equatorial plane and leaving at 22:50:42 UT when 160 km south. Spacecraft orientation was fixed throughout. Closest approach to the 1529-km-diameter moon's leading hemisphere occurred 228 km south of the equatorial plane, when Cassini was 1244 km downstream of Rhea's center. Points along the trajectory are separated by 5 min. The Cartesian coordinate system shown, displaced here and in other figures for clarity from its origin at Rhea's center, has components along Rhea's orbital motion vector (X), Saturnward (Y), and perpendicular to Rhea's orbital plane (Z).

[1]Max-Planck-Institut für Sonnensystemforschung, Max-Planck-Strasse 2, 37191 Katlenburg-Lindau, Germany. [2]Mullard Space Science Laboratory, Department of Space and Climate Physics, University College London, Holmbury St. Mary, Dorking, Surrey RH5 6NT, UK. [3]Centre for Planetary Sciences, University College London, London WC1E 6BT, UK. [4]Max Planck Institut für Kernphysik, Saupfercheckweg 1, 69117 Heidelberg, Germany. [5]Southwest Research Institute, Culebra Road, San Antonio, TX 78238, USA. [6]Centre d'Etude Spatiale des Rayonnements, Paul Sabatier University, Centre National de la Recherche Scientifique, 9 Avenue du Colonel Roche, Toulouse, 31400 France. [7]Astronomical Institute of St. Petersburg State University, Universitetskii pr. 28, Staryi Peterhof, St. Petersburg, 198504, Russia. [8]The Blackett Laboratory, Imperial College London, London SW7 2BW, UK. [9]Swedish Institute of Space Physics, Box 537, 751 21 Uppsala, Sweden. [10]Jet Propulsion Laboratory, California Institute of Technology, 4800 Oak Grove Drive, Pasadena, CA 91109, USA. [11]Department of Physics and Astronomy, The University of Iowa, Iowa City, Iowa 52242, USA. [12]Department of Materials Science and Engineering, University of Virginia, Post Office Box 400745, 116 Engineer's Way, Charlottesville, VA 22904, USA. [13]Institute of Geophysics and Planetary Physics, University of California, Los Angeles, 6863 Slichter Hall, Los Angeles, CA 90095, USA. [14]The Johns Hopkins University Applied Physics Laboratory, 11100 Johns Hopkins Road, Laurel, MD 20723, USA. [15]Academy of Athens, Soranou Efesiou 4, Athens 115 27, Greece. [16]Institut für Geophysik und Meteorologie, Universität zu Köln, Albertus-Magnus-Platz, 50923 Köln, Germany. [17]AG Nichtlineare Dynamik, Universität Potsdam, Postfach 601553, 14469 Potsdam, Germany. [18]Department of Earth and Planetary Science, The Johns Hopkins University, Baltimore, MD 21218, USA. [19]Los Alamos National Laboratory, Los Alamos, NM 87545, USA.

*To whom correspondence should be addressed. E-mail: ghj@mssl.ucl.ac.uk

in its equatorial plane, with orbital radii of ~1610, ~1800, and ~2020 km. The slight asymmetry in dip positions may be caused by a modest tilt to the local magnetic field.

The dips may instead represent the cumulative effect of material upstream of Cassini: Saturn's corotational plasma flows across the rings, rather than parallel to them as occurs at Saturn itself. The dips may therefore occur downstream of local maxima in ring column density presented to the corotating plasma, that is, the ansae, where narrow rings' tangents directly upstream of Cassini are parallel to the flow. For this scenario, assuming perfectly circular rings, common plasma flow deviations (*5*) could explain the slight asymmetry in the dips' locations. A further complication of both ring interpretations is the observed electrons' multiple traverses of the Hill sphere before detection. If an integer number of electron half bounce-lengths separates Cassini from a single ring, multiple "ghost" dips may form through occasional constructive interference of weaker depletions. Dust lofted by plasma-induced charging of Rhea's regolith (*13*) would have been a candidate nonring obstacle, especially as near-zero grain potentials at Rhea (*14*) may make its surface particularly sensitive to

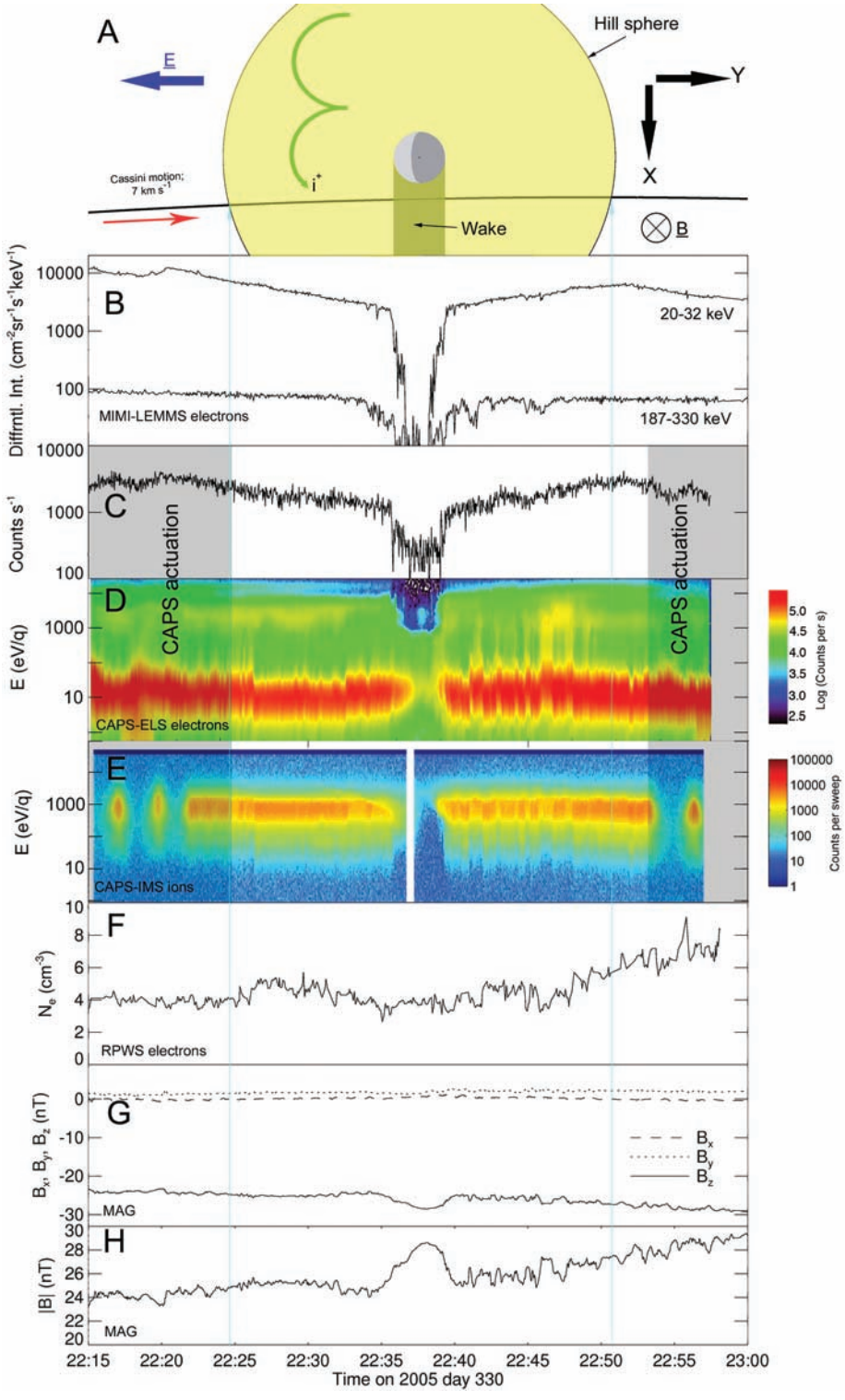

Fig. 2. Data returned during the flyby. (**A**) Rhea and its Hill sphere to the same scale as the other panels. The general directions of the local magnetic [B] and corotational electric [E] fields are shown, together with the initial gyromotion of a freshly created pickup ion, i^+. Prominent in almost all data sets is Rhea's infilling wake (22:35:30 to 22:39:40 UT). (**B**) MIMI (*19*) LEMMS 20 to 32 keV and 187 to 330 keV. keV electron fluxes at pitch angles ~10°. (**C**) CAPS (*20*), electron spectrometer (ELS) 26 keV electron fluxes at pitch angles of ~90°. (**D**) CAPS-ELS electron fluxes. (**E**) CAPS ion mass spectrometer (IMS) ion spectrogram (all anodes), showing gyroradius effects in Rhea's wake. (**F**) Total electron number density from RPWS (*21*) upper hybrid frequency values. (**G**) Components and (**H**) magnetic field magnitude from Cassini's magnetometer (*22*, *23*). Magnetic field variations appear consistent with Rhea being plasma-absorbing: The evacuated wake's field strength is enhanced to maintain constant total particle plus magnetic pressure. The magnetic field wave power decreases somewhat within the Hill sphere, probably due to charged particle loss causing decreased plasma β; otherwise, no direct magnetic field perturbations are convincingly evident on the Hill sphere's scale. Cassini's flyby trajectory, almost confined to the interaction region's equatorial symmetry plane, where field rotations are minimized, and almost transverse to the north-south symmetry plane, makes a decisive interpretation difficult.

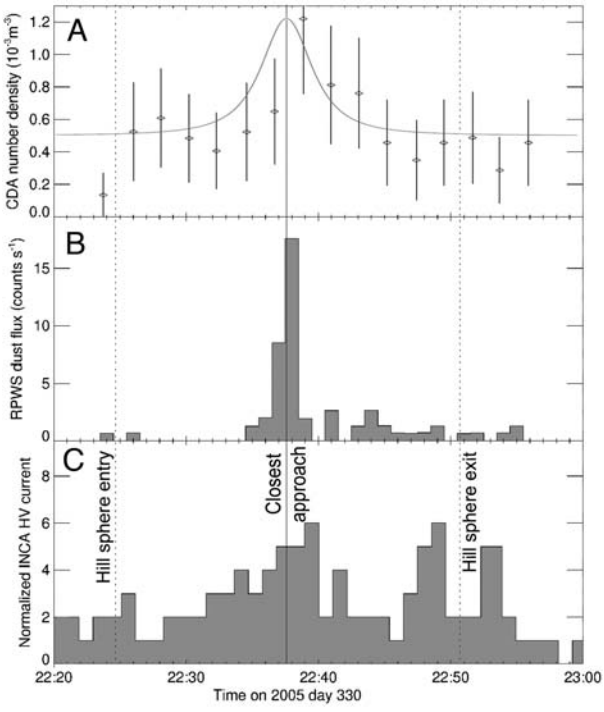

Fig. 3. In situ dust observations. (**A**) Comparison of recalibrated and dead time-corrected >1μm CDA data to a modeled isotropic impactor-ejecta number density (*1*). Two other instruments provide in situ dust data: RPWS (*21*) detects expanding plasma clouds resulting from high-velocity dust impacts onto Cassini (*24*), while MIMI-INCA (*19*) records dust-induced discharges between its collimating plates. (**B**) The RPWS dust flux, estimated to respond to particles >~3 μm. (**C**) MIMI-INCA high-voltage current. Although ultraviolet light may cause spurious signals in the INCA data set, dust impacts are believed to dominate.

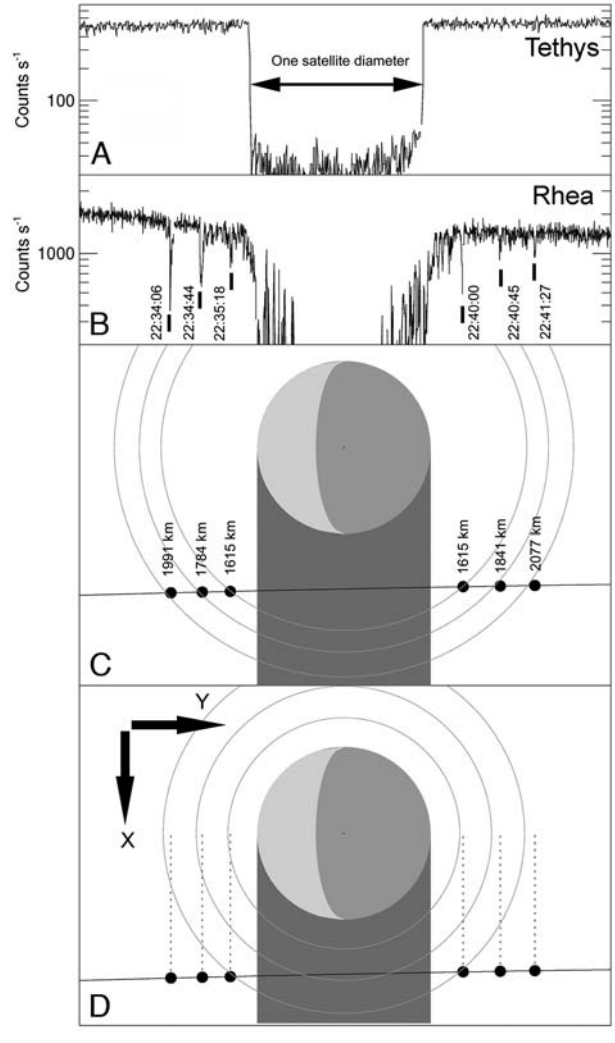

Fig. 4. Interpretation of electron flux dropouts as evidence of a ring system. (**A**) 28 to 49 keV electron fluxes at Tethys, demonstrating that moon's sharp, isolated absorption signature, in contrast to equivalent data from Rhea (**B**). The panels are scaled such that the relative size of the satellites' diameters is equal. Rhea's wake infills more rapidly because of the higher local plasma temperature. (**C**) Locations of some short-lived electron flux dropouts visible in the MIMI-LEMMS electron flux shown in (B). Their distances from Rhea's rotational axis are shown. Such absorptions, reminiscent of other planetary ring signatures (*25*), could be explained by the occultation of southward-traveling electrons before detection by Cassini. The signatures' spatial near-symmetry may signal the presence of three near-circular rings or arcs of material ~230 km north, in Rhea's equatorial plane. (**D**) An alternative dropout formation scenario.

such processes. However, several discrete sheets of grains as implied by multiple dips cannot be easily explained.

Numerical simulations imply that bodies that are subject only to minor perturbations by non-gravitational forces could orbit Rhea stably for long periods (*15*). Impacts on Rhea large enough to result in the orbit of ejecta material may have occurred as recently as 70 million years ago (*16*). Disruptive capture of a minor body is also possible. In these cases, some debris could have remained in orbits that flattened and circularized over time. Clumps of Rhea-orbiting material could maintain this disk, and bombardment by E-ring debris and extra-Saturnian grains would also release ejecta into near-circular orbits. Isolated clumps or moonlets could also explain the material's gravitational containment in discrete rings or arcs. Given their orbital stability, rings may even have survived since Rhea's formation.

References and Notes

1. A. V. Krivov *et al.*, *Planet. Space Sci.* **51**, 251 (2003).
2. M. Sremcevic, A. V. Krivov, F. Spahn, *Planet. Space Sci.* **51**, 455 (2003).
3. J. F. Carbary, S. M. Krimigis, W.-H. Ip, *J. Geophys. Res.* **88**, 8947 (1983).
4. Materials, methods, and further discussion are available as supporting material on *Science* Online.
5. G. H. Jones *et al.*, *Science* **311**, 1412 (2006).
6. R. Srama *et al.*, *Space Sci. Rev.* **114**, 465 (2004).
7. J. Saur, D. F. Strobel, *Astrophys. J.* **620**, L115 (2005).
8. L. W. Esposito *et al.*, *Space Sci. Rev* **115**, 299 (2004).
9. M. F. Thomsen, J. A. Van Allen, *J. Geophys. Res.* **85**, (A11), 5831 (1980).
10. National Institute of Standards and Technology Physical Reference Data, http://physics.nist.gov/PhysRefData/, (2006).
11. J. N. Cuzzi, J. A. Burns, *Icarus* **74**, 284 (1988).
12. P. C. Birch, S. Chapman, *Phys. Plasmas* **9**, 1785 (2002).
13. T. J. Stubbs *et al.*, abstr. 1899, *Lunar and Planetary Science Conference XXXVI*, Lunar and Planetary Institute (League City, TX, 14 to 18 March 2005).
14. S. Kempf *et al.*, *Planet. Space Sci.* **54**, 999 (2006).
15. Test particles were inserted into a wide range of simulated orbits about Rhea in the restricted three-body problem framework (*17*). Over >35,000 Saturnian years, semimajor axis, eccentricity, and inclination perturbations were remarkably restricted, as found in other contexts (*18*). Most <30° inclination particles survived the full, 10^6-year integration period if initial pericentres permitted small eccentricity excursions. Particles at the brief electron dropouts' distances were largely unperturbed. Overall stability was unchanged over a separate, 10^5-year integration that additionally included Titan's presence and Saturn's oblateness (*4*).
16. R. J. Wagner *et al.*, *Lunar and Planetary Science Conference XXXVIII*, abstr. 1958, Lunar and Planetary Institute (League City, TX, 12 to 16 March 2007).
17. E. Everhart, in *Dynamics of Comets: Their Origin and Evolution*, A. Carusi, B. Valsecchi, Eds. (D. Reidel, Dordrecht, Netherlands, 1985), pp. 185–202.
18. D. P. Hamilton, J. A. Burns, *Icarus* **92**, 118 (1991).
19. S. M. Krimigis *et al.*, *Space Sci. Rev.* **114**, 233 (2004).
20. D. T. Young *et al.*, *Space Sci. Rev.* **114**, 1 (2004).
21. D. A. Gurnett *et al.*, *Space Sci. Rev.* **114**, 395 (2004).
22. M. K. Dougherty *et al.*, *Space Sci. Rev.* **114**, 331 (2004).
23. K. K. Khurana, C. T. Russell, M. K. Dougherty, *Icarus* **192**, 465 (2008).
24. W. S. Kurth *et al.*, *Planet. Space Sci.* **54**, 988 (2006).
25. E. Roussos *et al.*, *Icarus* **193**, 455 (2008).

26. Cassini-Huygens is a mission of international collaboration between NASA, the European Space Agency (ESA), and the Agenzia Spaziale Italiana (ASI). We thank M. Kusterer (The Johns Hopkins University Applied Physics Laboratory, JHUAPL), N. Achilleos, and S. Kellock (Imperial College London) for data reduction. MIMI/LEMMS was partly financed by the German Bundesministerium für Bildung und Forschung through the German Aerospace Center (DLR) and by the Max Planck Gesellschaft. Work at JHUAPL, Johns Hopkins University, University of Iowa, and Southwest Research Institute was supported by NASA, as was that at Los Alamos National Laboratory, under the auspices of the U.S. DOE. Work at University College London and Imperial College London was supported by the U.K. Science and Technology Facilities Council. We acknowledge suggestions by T. V. Johnson and discussions with N. André and J. Schmidt.

Supporting Online Material
www.sciencemag.org/cgi/content/full/319/5868/1380/DC1
Materials and Methods
SOM Text
Figs. S1 to S9
References

9 October 2007; accepted 1 February 2008
10.1126/science.1151524

TOPLESS Mediates Auxin-Dependent Transcriptional Repression During *Arabidopsis* Embryogenesis

Heidi Szemenyei,[1,2] Mike Hannon,[1,2] Jeff A. Long[1]*

The transcriptional response to auxin is critical for root and vascular development during *Arabidopsis* embryogenesis. Auxin induces the degradation of AUXIN/INDOLE-3-ACETIC ACID (AUX/IAA) transcriptional repressors, freeing their binding partners, the AUXIN RESPONSE FACTOR (ARF) proteins, which can activate transcription of auxin response genes. We show that TOPLESS (TPL) can physically interact with IAA12/BODENLOS (IAA12/BDL) through an ETHYLENE RESPONSE FACTOR (ERF)–associated amphiphilic repression (EAR) motif. TPL can repress transcription in vivo and is required for IAA12/BDL repressive activity. In addition, *tpl-1* can suppress the patterning defects of the *bdl-1* mutant. Direct interaction between TPL and ARF5/MONOPTEROS, which is regulated by IAA12/BDL, results in a loss-of-function *arf5/mp* phenotype. These observations show that TPL is a transcriptional co-repressor and further our understanding of how auxin regulates transcription during plant development.

The phytohormone auxin has been implicated in many aspects of plant biology, including pattern formation during embryogenesis, lateral organ development, and cell expansion (*1*). Auxin mediates these activities through a signaling cascade involving AUXIN RESPONSE FACTORS (ARFs), which constitute a family of transcription factors that activate or repress expression of auxin response genes (*2*), and the AUX/IAA family of transcriptional repressors (*3*). AUX/IAAs negatively regulate auxin-mediated transcription by binding ARFs through conserved domains III and IV found in both types of proteins (*4*, *5*).

Domain II of AUX/IAAs interacts with the auxin receptor TRANSPORT INHIBITOR RESISTANT (TIR1), part of a Skp1/cullin/F-box protein (SCF) complex (*6*–*8*). Auxin stabilizes this interaction, leading to the degradation of AUX/IAAs and allowing ARFs to activate transcription. Mutations in AUX/IAAs that disrupt the interaction with the TIR1 protein family abolish their auxin-induced degradation (*8*). For example, *bodenlos-1* (*bdl-1*) contains a stabilizing mutation (P74S, substitution of proline 74 with serine) in *IAA12* (*9*). IAA12/BDL physically interacts with AUXIN RESPONSE FACTOR5/MONOPTEROS (ARF5/MP) and represses its activity (*9*). Consistent with this, both *bdl-1* mutants and loss-of-function *ARF5/MP* alleles display reduced vasculature and form a "basal peg" instead of a root and hypocotyl (the seedling stem) (*10*–*12*).

Although no prior connection has been made to auxin signaling, the most severe *topless-1* (*tpl-1*) phenotype, a homeotic transformation of the apical pole (the shoot) into a second basal pole (the root), suggests that it plays a role in this pathway (*13*). *tpl-1* is temperature sensitive and displays a range of phenotypes, all disrupting the patterning of the apical half of the embryo. The *tpl-1* mutation is a histidine substitution at asparagine 176 (N176H), and this allele acts as a dominant negative for the TOPLESS RELATED (TPR) family (*14*). On the basis of its domain structure and genetic interactions with a histone deacetylase and a histone acetyl transferase, TPL has been proposed to be a transcriptional co-repressor (*14*).

Transcriptional co-repressors do not bind DNA directly, but are recruited to DNA through interactions with DNA-binding transcription factors (*15*). Determining a co-repressor's binding partners can provide insight into its biological relevance. Therefore, we performed yeast two-hybrid screens to find protein interactors using full-length TPL or the N terminus of TPL (Fig. 1A). Multiple AUX/IAAs, including IAA12/BDL, were among the positive clones in both screens (table S2). IAA12/BDL contains the four conserved domains found in most AUX/IAAs (domains I to IV) (Fig. 1A). Through truncation analyses, we determined that domain I of IAA12/BDL is necessary and sufficient to interact with the C-terminal to lissencephaly homology (CTLH) domain of TPL (*16*) (Fig. 1, B and C).

Domain I of the AUX/IAAs contains an ERF-associated amphiphilic repression (EAR) motif (*17*), which is known to be involved in transcriptional repression (*18*). To determine if this motif is essential for the interaction with TPL, we tested an IAA12/BDL construct in which three leucines at the core of the EAR domain were changed to alanines (IAA12/BDL mEAR) (Fig. 1A). These changes to the EAR domain severely weakened the interaction between TPL and IAA12/BDL both in yeast two-hybrid assays (Fig. 1C) and assays in which glutathione *S*-transferase (GST)–tagged in vitro–translated products were used (Fig. 1D).

We also tested the interaction between IAA12/BDL and TPL using plant lysates. We found that column-bound GST-IAA12/BDL and GST-N-TPL could affinity purify TPL fused to a 6× hemagglutinin tag (TPL-HA) from plant extracts (Fig. 1E), whereas purified GST or beads alone could not, further indicating that TPL interacts with IAA12/BDL. These results also demonstrate that TPL can homodimerize, a characteristic shared with other transcriptional co-repressors (*19*). GST-N-TPL N176H could also pull down BDL P74S–green fluorescent protein (GFP) from plant lysates (Fig. 1F). Mutations in the EAR domain of GST-IAA12/BDL disrupted the interaction with TPL (Fig. 1E). These interactions were also observed in a tobacco transient expression system (*20*) by means of bimolecular fluorescence complementation (BiFC) (*21*) (fig. S2).

To investigate the biological significance of these physical interactions, we analyzed *tpl-1bdl-1* double mutants. *bdl-1* seedlings form a basal peg (Fig. 2C), lacking hypocotyl and root structures of wild-type seedlings (Fig. 2A), whereas *tpl-1* roots appear normal (Fig. 2B). *tpl-1bdl-1* seedlings formed hypocotyls and roots (Fig. 2D and table S3), indicating that *tpl-1* can suppress the basal patterning defects seen in *bdl-1*. *bdl-1* mutants also display a reduction in cotyledon (seed leaf) vasculature development (Fig. 2G). Wild-type and *tpl-1* cotyledons develop a primary midvein with loops of lateral veins along the margins (Fig. 2, E and F). In *bdl-1*, these veins are either absent or severely reduced (n = 70) (Fig. 2G) (*10*). Vasculature formation was

[1]Plant Biology Laboratory, The Salk Institute for Biological Studies, 10010 North Torrey Pines Road, La Jolla, CA 92037, USA. [2]Division of Biological Sciences, Section of Cell and Developmental Biology, University of California at San Diego, 9500 Gilman Drive, La Jolla, CA 92093, USA.

*To whom correspondence should be addressed. E-mail: long@salk.edu